American Mineralogist, Volume 73, pages 901–909, 1988

Convolution effect in the determination of compositional profiles and diffusion coefficients by microprobe step scans

Jibamitra Ganguly
Department of Geosciences, University of Arizona, Tucson, Arizona 85721, U.S.A.
Rabi N. Bhattacharya
Department of Mathematics, University of Indiana, Bloomington, Indiana 47401, U.S.A.
Sumit Chakraborty
Department of Geosciences, University of Arizona, Tucson, Arizona 85721, U.S.A.

Abstract

We present a mathematical formulation and numerical simulations that allow one to evaluate the convolution effect in the measurement of compositional or diffusion profiles due to spatial averaging in microprobe analysis. The analytical relation between the true and measured (convolved) compositions is reduced to a simple form that can be applied to calculate the convolution effect in microprobe step-scanning with the aid of an ordinary scientific calculator.

It is assumed that the excitation intensity of the sample volume has a Gaussian distribution with radial symmetry about the beam axis. The error standard deviation ϵ of the Gaussian, which is required to evaluate the convolution effect, can be determined by analyzing the smoothing of compositional discontinuity in a standard sample. The convolution effect on the measurement of a concentration profile vanishes when the latter has a constant slope and increases with the increase in the curvature of the profile. For a given value of ϵ, the calculated convolution of a diffusion profile with constant diffusion coefficient almost exactly agrees with that predicted from probability theory.

The convolution effect on a diffusion coefficient retrieved directly from an experimentally measured diffusion profile decreases with the increasing length and decreasing value of ϵ and is insignificant for a profile about 15 μm long in a modern electron microprobe. Our formulation should also prove useful in retrieving true composition near a grain boundary from a microprobe spot analysis that suffers from spatial averaging of compositions on both sides of the boundary.

Introduction

Precise measurement of compositional profiles in minerals, metallic alloys, and glasses is a problem of considerable interest in mineralogy, petrology, and geochemistry as well as in materials and solid-state sciences. The classical application of such measurements is in the field of diffusion studies. More recently, petrologists have been measuring compositional zoning in natural minerals in attempts to retrieve from these data their thermal and growth histories (e.g., Loomis, 1983).

The compositional zonings are usually measured by step-scanning of the sample in an electron, ion, or Auger microprobe. The composition that is measured by the electron or ion beam represents a weighted spatial average of the composition of the sample around the point of incidence of the beam. This convolution effect varies depending on the physics of the excitation process and instrumental factors, but is probably relatively strong in the case of electron-microprobe analysis.

We were led into the problem of analysis of the convolution effect as part of our continuing study on cation diffusion in garnet (Elphick et al., 1985; Loomis et al., 1985; Ganguly and Chakraborty, 1987). The work involved microprobe analysis of experimentally induced diffusion profiles in garnet-garnet diffusion couples. The diffusion profiles were extremely short in some cases (Elphick et al., 1985) so that the retrieval of diffusion parameters from these profiles required a proper understanding of the broadening effect due to spatial averaging in the microprobe spot analysis. A similar problem was faced by Lo and Schuele (1975), who developed an elaborate technique of deconvolution.

In this work, we present a theoretical analysis and numerical simulations of the convolution effect, which are much simpler than the previous formulations and should be of general interest in the problem of measurement of compositional zoning in minerals and other solids by spot analysis, and also in the retrieval of diffusion coefficients from such data. It should be noted that our treatment is applicable to the convolution problem in any type of microprobe (i.e., electron, ion, or Auger microprobe)—not just to that in the electron microprobe, which is commonly used by the geological community.

Goldstein and Colby (1975) suggested that since the deconvolution analysis is extremely difficult to perform, one may convolve hypothetical concentration profiles

0003–004X/88/0708–0901$02.00

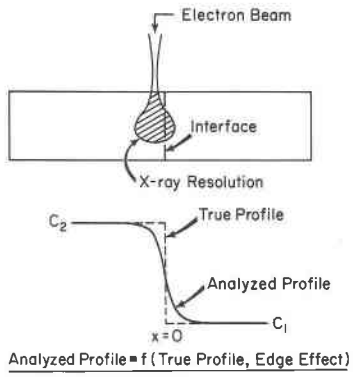

Fig. 1. Spatial averaging effect in the microprobe analysis of a concentration profile by step-scanning across an interface between two phases. The true profile is discontinuous at the interface, but when the electron (or ion) beam is near the interface, the excited sample volume involves compositions on both sides of the interface, thereby smoothing out the compositional discontinuity in the analysis of the concentration profile. (The distance coordinate X is equivalent to x_1 in the text.)

until a match is found with the observed profile and thus "predict" the true profile. They have developed a (computer-aided) numerical method to perform the convolution analysis. Below, we develop analytical formulations that serve the same purpose, but can be easily used to calculate the convolution effect with the aid of a scientific calculator (see example in App. 3). In addition, we also present an analytical relation from which one can directly calculate the error in the determination of the diffusion coefficient due to the convolution effect on the measurement of the diffusion profiles by step-scanning with a microprobe.

The spatial resolution of microprobe analysis will improve with time as more sophisticated instruments and techniques become available, but the convolution effect can never be completely avoided since the analysis involves excitation of a finite sample volume. Thus, a proper understanding of the convolution effect is essential to the evaluation and improvement of the *effective* resolution of microbeam analysis.

Mathematical formulations

General relation between true and convolved compositions

The effect of spatial averaging on the analysis of a compositional profile is illustrated schematically in Figure 1. This is a special case, in which the *true* concentration profile of an element is discontinuous at the interface of two samples, but each sample has a constant concentration of the element. However, the measured concentration profile will be continuous owing to the spreading of the electron beam and spatial averaging of compositions on both sides of the interface.

We make the usual assumption (e.g., Goldstein and Colby, 1975; Lo and Schuele, 1975) that the excitation of the sample volume has a Gaussian intensity distribution that is radially symmetric. In other words, the excitation intensity (or density) around the sample point is of the form

$$\bar{\phi}_\epsilon(\mathbf{x}) = \left(\frac{1}{\sqrt{2\pi}\epsilon}\right)^3 \exp\left(-\frac{x_1^2}{2\epsilon^2} - \frac{x_2^2}{2\epsilon^2} - \frac{x_3^2}{2\epsilon^2}\right), \tag{1}$$

where $\mathbf{x} = (x_1, x_2, x_3)$, and ϵ is an arbitrary positive parameter. It is well known, and simple to check, that for this intensity distribution the mean displacement is zero and the standard deviation is ϵ (or the variance is ϵ^2) in every direction.

We may also express Equation 1 as

$$\bar{\phi}_\epsilon(\mathbf{x}) = \left(\frac{1}{\epsilon}\right)^3 \phi\left(\frac{x_1}{\epsilon}\right)\phi\left(\frac{x_2}{\epsilon}\right)\phi\left(\frac{x_3}{\epsilon}\right), \tag{2}$$

where ϕ is the so-called standard normal (or Gaussian) density function in one dimension,

$$\phi(x) = \frac{1}{\sqrt{2\pi}}\exp\left(-\frac{x^2}{2}\right). \tag{3}$$

Thus, if $\mathbf{x} = (x_1, x_2, x_3)$ denotes a point in the sample volume where the true concentration is $C(\mathbf{x})$, then the observed concentration $f(\mathbf{x})$ at $\mathbf{x}$ may be represented by the convolution relation

$$\begin{aligned} f(\mathbf{x}) &= (C*\bar{\phi}_\epsilon)(\mathbf{x}) \\ &= \int_{-\infty}^{\infty}\int_{-\infty}^{\infty}\int_{-\infty}^{\infty} C(\mathbf{x}-\mathbf{y})\bar{\phi}_\epsilon(\mathbf{y})\,d\mathbf{y} \\ &= \int_{-\infty}^{\infty}\int_{-\infty}^{\infty}\int_{-\infty}^{\infty} C(\mathbf{x}+\mathbf{y})\bar{\phi}_\epsilon(\mathbf{y})\,d\mathbf{y} \\ &= \int_{-\infty}^{\infty}\int_{-\infty}^{\infty}\int_{-\infty}^{\infty} C(\mathbf{x}+\epsilon\mathbf{z})\bar{\phi}_1(\mathbf{z})\,d\mathbf{z}, \end{aligned} \tag{4}$$

where $\mathbf{y} = (y_1, y_2, y_3)$, $= \epsilon\mathbf{z}$, * is the usual symbol for convolution, and $\bar{\phi}_1(\mathbf{z}) = \phi(z_1)\phi(z_2)\phi(z_3)$ is the standard normal density in *three dimensions*. We have suppressed the dependence of C on t above, as it is not needed for the analysis of the convolution effect.

If Δ is the spacing between two successive points in the spot analysis, then Equation 4 can be approximately written in terms of the summation relation

$$\begin{aligned} f(\mathbf{x}) = \sum_n \sum_{m=-\infty}^{\infty} \sum_r & C[\mathbf{x} + (n\Delta, m\Delta, r\Delta)] \\ & \cdot\phi\left(\frac{n\Delta}{\epsilon}\right)\phi\left(\frac{m\Delta}{\epsilon}\right)\phi\left(\frac{r\Delta}{\epsilon}\right)\left(\frac{\Delta}{\epsilon}\right)^3. \end{aligned} \tag{5}$$

Here each summation is from $-\infty$ to ∞, and $C[\mathbf{x} + (n\Delta, m\Delta, r\Delta)]$ is the true composition at $[\mathbf{x} + (n\Delta, m\Delta, r\Delta)]$. However, the tail probability of the Gaussian distribution is negligible beyond three or four times the standard de-

viation. Thus, for all practical purposes, one may take

$$f(\mathbf{x}) \approx \sum_{n} \sum_{\substack{m \\ =-\alpha}}^{\alpha} \sum_{r} C[\mathbf{x} + (n\Delta, m\Delta, r\Delta)] \cdot \phi\left(\frac{n\Delta}{\epsilon}\right)\phi\left(\frac{m\Delta}{\epsilon}\right)\phi\left(\frac{r\Delta}{\epsilon}\right)\left(\frac{\Delta}{\epsilon}\right)^3, \quad (6)$$

where each summation is from $-\alpha$ to α, with $\alpha = 4(\epsilon/\Delta)$, rounded off to the nearest integer.

For a physical understanding of the effect of convolution, we rewrite Equation 4 in the following form by expanding the function $C(\mathbf{x} - \mathbf{y})$ in a Taylor series around $\mathbf{x}$.

$$\begin{aligned} f(\mathbf{x}) &= \int_{-\infty}^{\infty}\int_{-\infty}^{\infty}\int_{-\infty}^{\infty} C(\mathbf{x} - \mathbf{y})\bar{\phi}_\epsilon(\mathbf{y})\, d\bar{\mathbf{y}} \\ &= \int_{-\infty}^{\infty}\int_{-\infty}^{\infty}\int_{-\infty}^{\infty}\Bigg[C(\mathbf{x}) - y_1\frac{\delta C(\mathbf{x})}{\delta x_1} \\ &\qquad - y_2\frac{\delta C(\mathbf{x})}{\delta x_2} - y_3\frac{\delta C(\mathbf{x})}{\delta x_3} \\ &\qquad + \tfrac{1}{2}\sum_{i,j=1}^{3} y_i y_j \frac{\delta^2 C(\mathbf{x})}{\delta x_i \delta x_j} \\ &\qquad - \cdots\Bigg]\bar{\phi}_\epsilon(\mathbf{y})\, d\mathbf{y}. \end{aligned} \quad (7)$$

Now $y_i\bar{\phi}_\epsilon(\mathbf{y})$ is an odd function of y_i; therefore, its integral vanishes. For the same reason, integrals of all terms $y_i y_j y_k \bar{\phi}_\epsilon(\mathbf{y})$ vanish, as do the integrals of terms like $y_1 y_2 \bar{\phi}_\epsilon(\mathbf{y})$, $y_1 y_3 \bar{\phi}_\epsilon(\mathbf{y})$, and $y_2 y_3 \bar{\phi}_\epsilon(\mathbf{y})$. Therefore, recalling that the variance of each coordinate under $\bar{\phi}_\epsilon$ is ϵ^2, while fourth moments are of the order ϵ^4, one gets

$$f(\mathbf{x}) = C(\mathbf{x}) + \frac{\epsilon^2}{2}\left[\frac{\delta^2 C(\mathbf{x})}{\delta x_1^2} + \frac{\delta^2 C(\mathbf{x})}{\partial x_2^2} + \frac{\delta^2 C(\mathbf{x})}{\delta x_3^2}\right] + O(\epsilon^4), \quad (8)$$

where the remainder term $O(\epsilon^4)$ is of the order of ϵ^4 and may be neglected. It is evident from Equation 8 that the convolution effect vanishes when the true profile has a constant slope and increases with the increase in the curvature of the concentration profile if terms of the order ϵ^4 may be neglected, as is usually the case.

Let us now suppose, as a special case, that the concentration C varies only along one direction, x_1. This is the usual form of spatial dependence of C in a diffusion-couple experiment. Then one may simply write $C(x_1)$ for $C(\mathbf{x})$ and integrate the variables z_2, z_3 in the last expression in Equation 4 to get

$$f(\mathbf{x}) = \int_{-\infty}^{\infty} C(x_1 + \epsilon z_1)\phi(z_1)\, dz_1. \quad (9)$$

In particular, since $f(\mathbf{x})$ does not vary with x_2 and x_3, we may simply write it as $f(x_1)$. Equation 6 then becomes

$$f(x_1) \approx \sum_{n=-\alpha}^{\alpha} C(x_1 + n\Delta)\cdot\phi(n\Delta/\epsilon)\cdot\frac{\Delta}{\epsilon}, \quad (10)$$

where α is as defined in Equation 6, i.e., $\alpha = 4(\epsilon/\Delta)$. Similarly, Equation 8 becomes

$$f(x_1) \approx C(x_1) + \frac{\epsilon^2}{2}C''(x_1). \quad (11)$$

According to Equation 3, $\phi(-x) = \phi(x)$. Thus, for example, if $\alpha = 4$, then Equation 10 reduces to

$$\begin{aligned} f(x_1) \approx \{&\phi(4\Delta/\epsilon)[C(x_1 - 4\Delta) + C(x_1 + 4\Delta)] \\ &+ \phi(3\Delta/\epsilon)[C(x_1 + 3\Delta) + C(x_1 - 3\Delta)] \\ &+ \cdots + \phi(0)C(x_1)\}(\Delta/\epsilon). \end{aligned} \quad (12)$$

Equation 11 or 12 can then be evaluated easily to obtain the convolved composition $f(x_1)$ from the true composition $C(x_1)$ if the standard deviation ϵ of the Gaussian intensity distribution is known. From a practical point of view, ϵ may be determined from the convolution effect on a discontinuous profile (Fig. 1) in a control sample whose structural and chemical characteristics are similar to those of the sample of interest, provided that the spot analyses have been carried out under identical instrumental conditions in both cases.

Let $x_1 = 0$ be the point of discontinuity of the concentration profile in a control sample (Fig. 1), and

$$\begin{aligned} C(x_1) &= C_1 \quad \text{for} \quad x_1 > 0 \\ C(x_1) &= C_2 \quad \text{for} \quad x_1 \le 0. \end{aligned} \quad (13)$$

It can then be shown (see App. 1), using the convolution Equation 9, that

$$\epsilon = \frac{C_1 - C_2}{\sqrt{2\pi}\, f'(0)} \quad (14)$$

where $f'(0)$ is the slope of the convolved or measured concentration profile in the control sample at $x_1 = 0$, and $C_2 > C_1$.

Convolution effect on diffusion profile and diffusion coefficient

In this section, we treat the relatively simple case that the diffusion coefficient is independent of composition. If the discontinuous concentration profile illustrated in Figure 1 is now allowed to relax by diffusion, then the concentration $C(x_1,t)$ is given by (Crank, 1975)

$$C(x_1,t) - C_1 = \frac{C_o}{2}\left[1 - \operatorname{erf}\left(\frac{x_1}{2\sqrt{Dt}}\right)\right] \quad (15)$$

where $C_o = C_2 - C_1$, D is the diffusion coefficient, and

$$\operatorname{erf}(z) = \frac{2}{\sqrt{\pi}}\int_0^z e^{-\eta^2}\, d\eta. \quad (16)$$

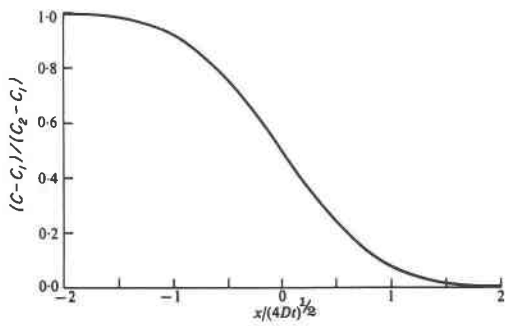

Fig. 2. Diffusion profile of a species with constant diffusion coefficient in a diffusion-couple experiment. The interface is at X (or x_1) = 0. The normalized concentration is plotted against the dimensionless parameter $X/\sqrt{4Dt}$. The initial concentration is equivalent to the "true profile" in Figure 1. The concentration C of the diffusing component varies between C_2 and C_1.

The diffusion profile described by Equation 15 is illustrated in Figure 2. It follows from Equations 15 and 16 (see App. 2) that

$$C''(x_1) = \frac{2C_o x_1 e^{-(x_1/k)^2}}{k^3\sqrt{\pi}}, \tag{17}$$

where $k = 2\sqrt{Dt}$. Thus, from Equations 11 and 17, and neglecting higher-order terms,

$$\frac{f(x_1) - C_1}{C_o} \approx \frac{C(x_1) - C_1}{C_o} + \left[\frac{x_1 e^{-(x_1/k)^2}}{k^3\sqrt{\pi}}\right]\epsilon^2. \tag{18}$$

The second term on the right, which is due to the convolution effect, vanishes at $x_1 = 0$, that is, at the interface of the diffusion couple.

The convolution of the diffusion profile will evidently lead to an estimation of diffusion coefficient that is larger than its true value unless the effect of convolution is corrected for. The observed concentration distribution is the convolution of the true concentration profile and the error distribution. Now the convolution of two independent Gaussian distributions is a Gaussian distribution whose variance (or mean square displacement) is the sum of variances of its components. From probability theory, $2Dt$ is the variance of a diffusion profile characterized by a constant diffusion coefficient (e.g., Shewmon, 1963, p. 53), such as given by Equation 15. Therefore,

$$2D_c t = 2Dt + \epsilon^2, \tag{19}$$

where $2D_c t$ is the variance of the Gaussian error distribution of the measured concentration profile, or in other words, D_c is the diffusion coefficient that would be directly retrieved from the measured concentration profile. From Figure 2, the half-length of the measured concentration profile, x_c, is given by $x_c = 4\sqrt{D_c t}$. Thus, from Equation 19, we obtain

$$D/D_c = 1 - 8(\epsilon/x_c)^2. \tag{20}$$

This relation among D/D_c, half-width of the diffusion profile, and ϵ is illustrated in Figure 3. As we shall see later, the ϵ values obtainable with electron microprobes do not usually exceed 0.6 μm. For ϵ = 0.6 μm, the diffu-

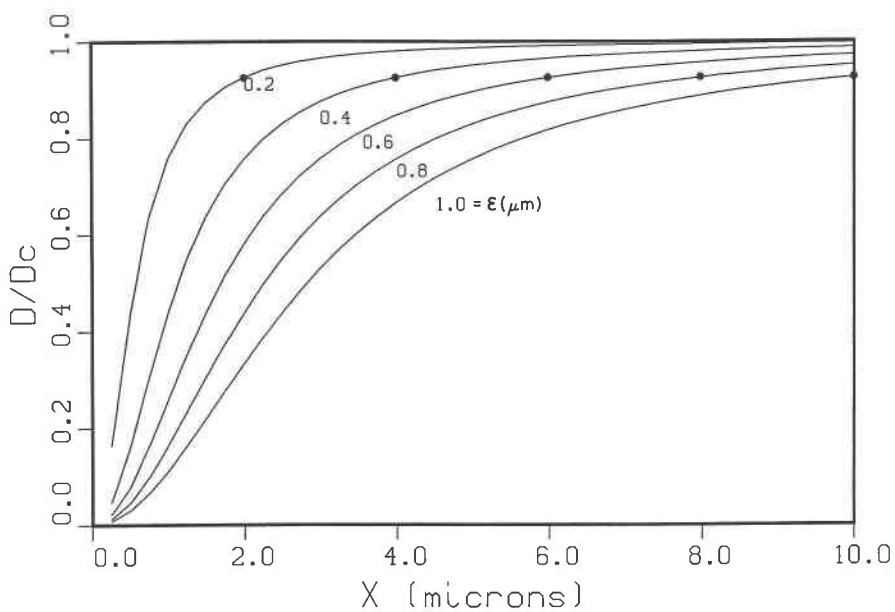

Fig. 3. Illustration of the convolution effect on the determination of a diffusion coefficient from concentration profiles measured with a microprobe. D is the true diffusion coefficient whereas D_c is the diffusion coefficient that would correspond to the convolved diffusion profile (see Fig. 5). ϵ is the assumed standard deviation of the Gaussian error function density of the excited sample volume, and X is the half-length of a diffusion profile of a species with constant diffusion coefficient. The points on the curve illustrate D/D_c values corresponding to $X = 10\epsilon$ (see text and Fig. 5).

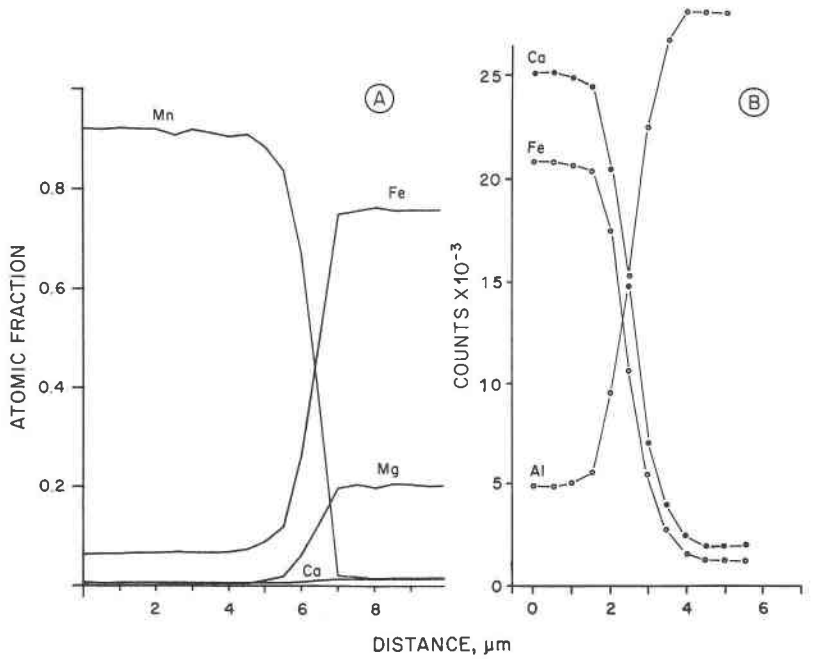

Fig. 4. Convolution effect on the electron-microprobe analysis of concentration profiles across interface of (**A**) spessartine-almandine and (**B**) almandine-Al couples (reproduced from Elphick et al., 1985). The true profiles are effectively discontinuous at the interface, which is at $X = 6.27$ μm. The spessartine-almandine couple was annealed at 30 kbar to 1200 °C for 2.5 h and to 800 °C for 9.5 h; the almandine-Al couple was made by inserting a piece of almandine in molten Al and quenching immediately. The analysis was done by step-scanning in an ARL microprobe at 0.5-μm intervals using 15-kV accelerating voltage and 50-nA beam current. Variations of voltage and current settings did not significantly affect the resolution (see text). The spot analysis around 7-μm distance in (A) must be slightly off in terms of composition as it produces too sharp a change in the curvature of the concentration profiles compared with that in the left side of the profiles and in the concentration profiles in (B).

sion coefficient retrieved directly from a 14-μm diffusion profile will be subjected to an 8% error, which is usually considered to be small or negligible, compared to various other uncertainties, in the determination of the diffusion coefficient. However, for profiles of smaller lengths, the error may be significant, and needs to be corrected for.

Numerical simulation of convolution effects

In this section, we present numerical simulation of the convolution effects in the determination of concentration profiles, in order to provide visual illustration of the mathematical formulations developed above and to convey a general idea of the situations where the broadening of the compositional profiles due to spatial averaging in spot analysis becomes important.

To obtain a value of ϵ that may be commonly encountered in microprobe analysis, we use the data of Elphick et al. (1985), who have step-scanned a garnet-garnet couple and a garnet–Al metal couple with very sharp compositional changes at the interface in an ARL (SEMQ) microprobe. Their results are reproduced here as Figure 4. The *true* compositional profiles may be treated as effectively discontinuous at the interface of each couple, the smoothing effect (due to a very small amount of diffusion at the annealing conditions) being negligible (Elphick et al., 1985). Using Equation 14, we obtain $\epsilon \approx 0.58$ μm; both samples yield essentially the same value of ϵ.

Elphick et al. (1985) performed these microprobe analyses with beam conditions of 15 kV and 50 nA. However, they stated that step-scanning at 10- and 20-nA beam currents at both 15- and 20-kV accelerating voltages did not significantly improve the analytical resolution of the concentration profiles. These additional analyses were performed across the garnet-garnet couple. We have performed further analysis of the garnet–Al metal couple using a beam current of 10 nA and an accelerating voltage of 11 kV. These results do not show any improvement of resolution. Therefore, we conclude that the variation of the analytical condition (within the normal operating ranges) at least in an ARL microprobe does not significantly affect the central part of the Gaussian of the X-ray intensity distribution, which effectively determines the extent of the spatial averaging. However, analysis of the garnet-garnet couple in a PHI600 model scanning Auger microprobe (SAM) resulted in a marked improvement of resolution, with ϵ around 0.25 μm (M. F. Hochella, Jr., A. M. Turner, and J. Ganguly, unpub. data). A comparison of the electron-microprobe and SAM scans of the garnet-garnet couple can be found in Hochella et al. (1986). It also seems likely that the resolution of the Auger analysis can be improved significantly.

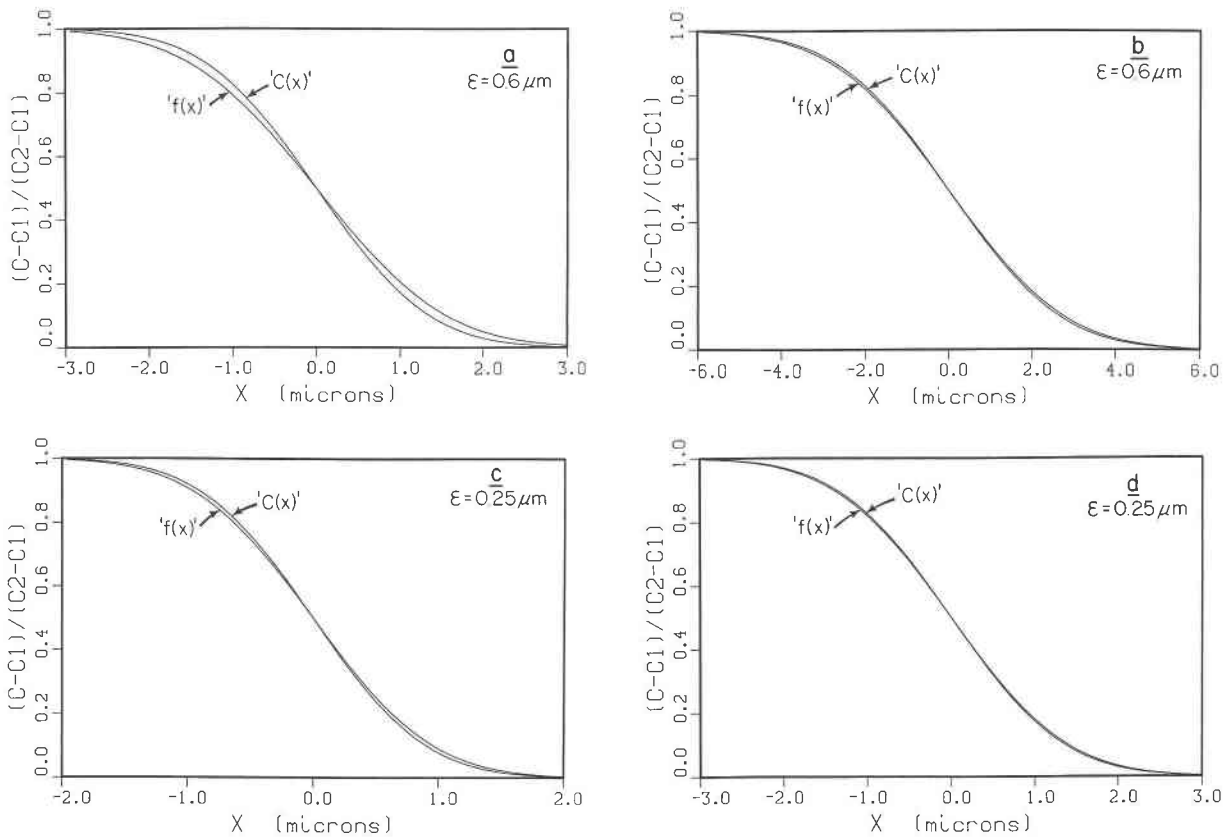

Fig. 5. Numerical simulation of convolution effects in the determination of diffusion profiles by microprobe spot analysis for different values of the error standard deviation (ϵ) and profile lengths. X = half-length of the profile; a couple interface is located at $X = 0$. "$C(x)$" and "$f(x)$" are true and convolved diffusion profiles, respectively, normalized to vary between 0 and 1. The diffusion coefficient is assumed to be constant in each profile. Two profile lengths are shown (left- and right-hand plots) for each value of ϵ.

Figure 5 shows numerical simulations of the convolution effects on diffusion profiles according to the mathematical formulations and ϵ values discussed above. Figures 5a and 5b are for $\epsilon = 0.6$ μm, whereas 5c and 5d are for $\epsilon = 0.25$ μm; x is half of the total length of the diffusion zone, which is bisected at the interface, $x = 0$. The numerical solutions obtained from the two alternative formulations of $f(x_1)$ (Eqs. 11 and 12) are virtually the same. For the specific concentration profile considered here, Equation 11 reduces to Equation 18. Calculations incorporating the ϵ^4 term did not result in any significant change of $f(x_1)$. Equation 12 is, in principle, more exact, but Equations 11 or 18 may be used to obtain essentially the same result if it proves to be advantageous from a computational point of view in certain situations.

The diffusion profiles in Figure 5 have been constructed by first choosing the maximum half-length of the profile and equating that to $4\sqrt{Dt}$ (Fig. 2). This gives the value of Dt for the calculation of a diffusion profile of desired length, which is then convolved according to Equations 11 and 12. Note in Figure 5 that the convolution effect almost vanishes when the half-length of the diffusion profile is about 10 times the value of ϵ. This is compatible with the probabilistic analysis of convolution effect on diffusion, which is illustrated in Figure 3 (in which the D/D_c values at $x = 10\epsilon$ are shown as points on the appropriate curves).

As a test of the method developed above, we simulate the convolution effect in the analysis of the discontinuous concentration profile of Mn across the garnet-garnet interface discussed above (Fig. 4A). Using $\epsilon = 0.58$ μm, as discussed above, and Equation 12, we obtain a convolved concentration profile (Fig. 6) that agrees very well with the results of the microprobe analyses. In the calculation of the convolution effect, the interface is assumed to equally divide a 0.5-μm step so that the convolution is symmetrical to the interface. This procedure approximately simulates the step-scanning in the microprobe in which care was taken not to analyze the interface per se while maintaining the 0.5-μm step size in an automated mode. Consequently, the interface is assumed to intersect a (convolved) concentration profile at a composition that

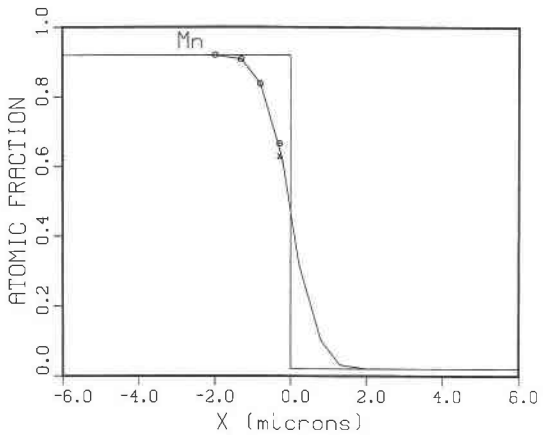

Fig. 6. Comparison of the simulated convolution in the analysis of the discontinuous Mn concentration profile of Figure 4A with the results of the corresponding microprobe spot analyses. The analytical data, shown as circled points, are from Figure 4A; data on only one side of the couple are shown as the convolution effect is symmetric on the two sides with respect to the interface and one of the analyzed points on the right side is slightly off-composition (see caption of Fig. 4). The concentration profile is constructed by joining convolved compositions, calculated at 0.5-μm steps, with the interface symmetrically dividing a step. Calculation of the point to the left of the interface, shown by a cross, is illustrated in Appendix 3.

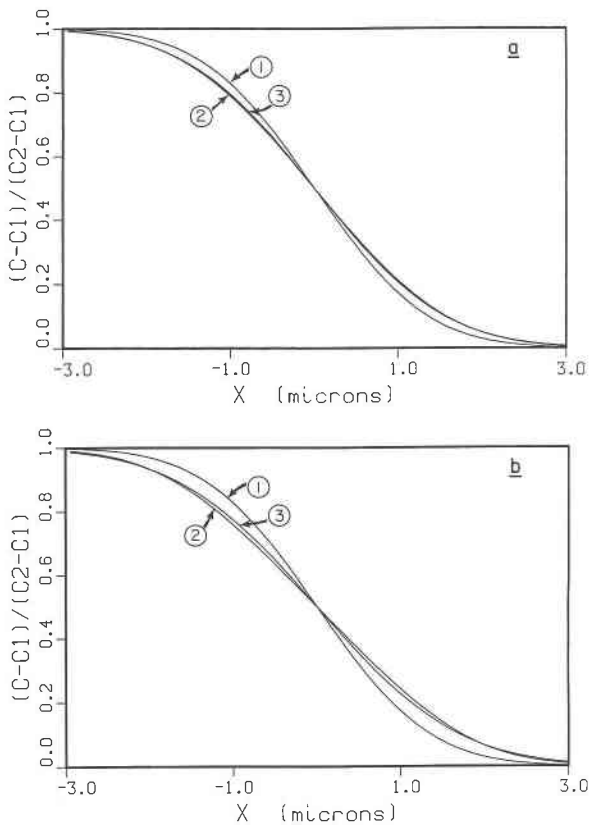

Fig. 7. Comparison of convolution effects in the microprobe analysis of a diffusion profile predicted by Equations 12 and 19. (**a**) Curve 1—diffusion profile for a constant value of the diffusion coefficient (Eq. 15); curve 2—numerical simulation of convolution of the diffusion profile for $\epsilon = 0.6$ μm according to Equation 12; curve 3—diffusion profile calculated directly from the convolution of diffusion coefficient given by Equation 19 and solution to the diffusion equation with constant diffusion coefficient (Eq. 15). (**b**) Curves have the same meaning as in (a), with $\epsilon = 0.8$ μm; curves 2 and 3 cross at $x = 0$.

equals $C_1 + (C_2 - C_1)/2$ ($C_2 > C_1$). The interface is, thus, located at $x \approx 6.27$ μm in Figure 4A.

For further illustration of the validity of the mathematical relation between the true and convolved compositions, we have compared in Figure 7 the numerical simulation of the convolution effect on a diffusion profile (according to Eq. 12) with that calculated analytically (according to Eq. 15) from the convolved diffusion coefficient D_c (Eq. 19). There is very good agreement between the two types of calculation of the convolution effect. The small disagreement at $\epsilon = 0.8$ μm is due to the accumulation of numerical errors.

The method developed above may be adapted to retrieve the true concentration profile from microbeam analyses near a grain boundary, where the measured profile suffers from spatial averaging of compositions on both sides of the boundary. This adaptation will be an iterative process involving convolution of hypothetical initial concentration profiles until a satisfactory match is found with the measured profile.

Acknowledgments

We are grateful to Michael Drake and Tom Teska for discussions and help with the microprobe analyses and to John Jones and Joaquin Ruiz for their comments on the manuscript. Constructive reviews by the Associate Editor Michael Hochella and two anonymous reviewers were very helpful in improving the clarity and organization of the paper. This research was supported by a grant from the U.S. National Science Foundation EAR-8417929.

References cited

Crank, J. (1975) The mathematics of diffusion (2nd ed.). Clarendon Press, Oxford.

Elphick, S.C., Ganguly, J., and Loomis, T.P. (1985) Experimental determination of cation diffusivities in aluminosilicate garnets: I. Experimental methods and interdiffusion data. Contributions to Mineralogy and Petrology, 90, 36–44.

Ganguly, J., and Chakraborty, S. (1987) Multicomponent cation diffusion and relaxation of compositional zoning in natural garnets. Geological Society of America Abstracts with Programs, 19, 671.

Goldstein, J.J., and Colby, J.W. (1975) Special techniques in the x-ray analyses of samples. In J.J. Goldstein and H. Yakowitz, Eds., Analytical scanning electron microscopy, 582 p. Plenum Press, New York.

Hochella, M.F., Jr., Turner, A.M., and Harris, D.W. (1986) High resolution scanning Auger microscopy of mineral surfaces. Scanning Electron Microscopy, 1986, 337–349.

Lo, C.C., and Schuele, D.E. (1975) Beam-diameter correction of x-ray intensity profile over small diffusion zones. Journal of Applied Physics, 46, 5004–5009.

Loomis, T.P. (1983) Compositional zoning of crystals: A record of growth

and reaction history. In S.K. Saxena, Ed., Advances in physical geochemistry, vol. 3, p. 1–60. Springer-Verlag, Berlin.

Loomis, T.P., Ganguly, J., and Elphick, S.C. (1985) Experimental determination of cation diffusivities in aluminosilicate garnets: II. Multicomponent simulation and tracer diffusion coefficients. Contributions to Mineralogy and Petrology, 90, 45–51.

Shewmon, P.G. (1963) Diffusion in solids, 203 p. McGraw-Hill, New York.

Manuscript received October 5, 1987
Manuscript accepted March 9, 1988

Appendix 1. Derivation of Equation 14 for ϵ

Since the initial concentration profile is one-dimensional in nature, we present below a derivation for the case of one-dimensional convolution, with ϕ_ϵ given by (for brevity, we use $x = x_1$, $y = y_1$, and $z = z_1$)

$$\phi_\epsilon(x) = \frac{1}{\epsilon}\phi(x/\epsilon) = \frac{1}{\epsilon\sqrt{2\pi}} e^{-x^2/2\epsilon^2}. \tag{1.1}$$

Using

$$C(x) = \begin{matrix} C_2 \text{ for } x \le 0 \\ C_1 \text{ for } x > 0 \end{matrix} \tag{1.2}$$

one has

$$\begin{aligned} f(x) &= \int_{-\infty}^{\infty} C(x - y')\phi_\epsilon(y')\, dy' \\ &= \int_{-\infty}^{\infty} C(y)\phi_\epsilon(x - y)\, dy, \ (y = x - y'). \end{aligned} \tag{1.3}$$

Since

$$\frac{d}{dx}[\phi_\epsilon(x - y)] = -\frac{1}{\epsilon^2}(x - y)\phi_\epsilon(x - y), \tag{1.4}$$

one obtains

$$\begin{aligned} f'(x) &= \frac{d}{dx} f(x) \\ &= \int_{-\infty}^{\infty} C(y)\left(-\frac{x - y}{\epsilon^2}\right)\phi_\epsilon(x - y)\, dy. \end{aligned} \tag{1.5}$$

Thus,

$$\begin{aligned} f'(0) &= \int_{-\infty}^{\infty} C(y)(y/\epsilon^2)\phi_\epsilon(-y)\, dy \\ &= \int_{-\infty}^{0} \cdots dy + \int_{0}^{\infty} \cdots dy \\ &= C_2 \int_{-\infty}^{0} (y/\epsilon^2)\phi_\epsilon(-y)\, dy \\ &\quad + C_1 \int_{0}^{\infty} (y/\epsilon^2)\phi_\epsilon(-y)\, dy \\ &= -C_2 \int_{0}^{\infty} (z/\epsilon^2)\phi_\epsilon(z)\, dz \\ &\quad + C_1 \int_{0}^{\infty} (y/\epsilon^2)\phi_\epsilon(y)\, dy, \quad (z = -y) \\ &= [(C_1 - C_2)/\epsilon^2] \int_{0}^{\infty} y\phi_\epsilon(y)\, dy. \end{aligned} \tag{1.6}$$

The last integral may be evaluated as follows:

$$\begin{aligned} \int_0^\infty y\phi_\epsilon(y)\, dy &= \int_0^\infty y\cdot(1/\epsilon)\phi(y/\epsilon)\, dy \\ &= \epsilon \int_0^\infty z\phi(z)\, dz \\ &= \frac{\epsilon}{\sqrt{2\pi}} \int_0^\infty z e^{-z^2/2}\, dz \\ &= \frac{\epsilon}{\sqrt{2\pi}} \int_0^\infty e^{-z^2/2} d\left(\frac{z^2}{2}\right) \\ &= \frac{\epsilon}{\sqrt{2\pi}} [-e^{-z^2/2}]_0^\infty \\ &= \frac{\epsilon}{\sqrt{2\pi}}. \end{aligned} \tag{1.7}$$

Thus we obtain

$$\epsilon = (C_1 - C_2)/[\sqrt{2\pi}\, f'(0)]. \tag{1.8}$$

Appendix 2. Derivation of Equation 17 for $C''(x)$

Let $J(p) = \mathrm{erf}(p)$ and $p = x/2\sqrt{Dt} = x/k$ ($x \equiv x_1$). Then from Equation 16

$$J'(p) = (2/\sqrt{\pi})e^{-p^2}. \tag{2.1}$$

Thus,

$$\frac{dJ(p)}{dx} = J'(p)\frac{dp}{dx} = \frac{2e^{-(x/k)^2}}{k\sqrt{\pi}} \tag{2.2}$$

and

$$\frac{d^2J(p)}{dx^2} = -\frac{4xe^{-(x/k)^2}}{k^3\sqrt{\pi}}. \tag{2.3}$$

We then have from Equation 15

$$\begin{aligned} C''(x) &= -\frac{C_o}{2}\left(\frac{d^2J(p)}{dx^2}\right) \\ &= \frac{2C_o x e^{-(x/k)^2}}{k^3\sqrt{\pi}}. \end{aligned} \tag{2.4}$$

Appendix 3. Illustration of the Application of Equation 12 to Calculate the Convolution Effect in Microprobe Spot Analysis

Let us first consider the Mn profile in Figure 4 for the calculation of the value of ϵ according to Equation 14. Since the true concentration profile is known to be discontinuous at the interface, the observed smoothing of the profile in the microprobe spot analysis can be used to calculate ϵ for the given analytical condition. In Equation 13, $f'(0)$ is the slope of the measured concentration profile (with respect to increasing distance) at the point of discontinuity of the true profile, which is the interface in Figure 4, and is located at $X = 6.27$ μm. Thus $f'(0) = -0.62$ μm^{-1}, whereas $C_2 = 0.92$ and $C_1 = 0.02$. Consequently,

$$\epsilon = \frac{0.02 - 0.92}{(\sqrt{2\pi})(-0.62)} = 0.58\ \mu\text{m}. \tag{3.1}$$

Let us now calculate the expected concentration of Mn in the microprobe spot analysis at 0.23 μm to the left of the interface. For convenience of reference, we translate the X axis so that the interface is set at $X = 0$. Then the above point is at $X = -0.23$ μm. The concentration profiles in Figure 4 have been determined by step-scanning at 0.5-μm intervals. Thus, according to Equation 6, $\alpha = 4(\epsilon/\Delta) = 4.6$, which may be rounded off to 5. We then have from Equation 10 or 12

$$f(x_1) \equiv f(-0.23\ \mu\text{m}) = \{\phi(5\Delta/\epsilon)[C(x_1 - 5\Delta) + C(x_1 + 5\Delta)] + \phi(4\Delta/\epsilon)[C(x_1 - 4\Delta) + C(x_1 + 4\Delta)] + \cdots + \phi(0)C(x_1)\}(\Delta/\epsilon). \quad (3.2)$$

From the expression of ϕ given by Equation 3,

$$\phi(5\Delta/\epsilon) \equiv \phi(3.448) = (1/\sqrt{2\pi})\exp[-(3.448)^2] = 2.7(10^{-6}), \quad (3.3)$$

and, similarly, $\phi(4\Delta/\epsilon) = 0.00054$, $\phi(3\Delta/\epsilon) = 0.00968$, and so on. For the Mn profile in Figure 4, $C(x_1 - m\Delta) = C(x_1) = 0.92$ whereas $C(x_1 + m\Delta) = 0.02$, where m is a positive integer between 1 and α, i.e., $1 \leq m \leq 5$. Substitution of the Δ, ϵ, and C values into Equation 3.2 yields (Fig. 6)

$$f(-0.23\ \mu\text{m}) = [0.0000027(0.92 + 0.02) + 0.00054(0.92 + 0.02) + 0.00968(0.92 + 0.02) + \cdots + (1/\sqrt{2\pi})(0.92)](0.50/0.58) = 0.63. \quad (3.4)$$